

Cite this article as: Li Jianbo, Wan Gang, Wu Bo, et al. Phase Stability and Aging Strengthening of  $Ti_2ZrNbV$  High Entropy Alloy[J]. Rare Metal Materials and Engineering, 2023, 52(04): 1184-1191.

ARTICLE

# Phase Stability and Aging Strengthening of $Ti_2ZrNbV$ High Entropy Alloy

Li Jianbo<sup>1</sup>, Wan Gang<sup>1</sup>, Wu Bo<sup>2</sup>, Xu Zaidong<sup>1</sup>, Man Jiale<sup>3</sup>, Zhang Lu<sup>1</sup>, Wu Baolin<sup>1</sup>

<sup>1</sup>Shenyang Aerospace University, Shenyang 110036, China; <sup>2</sup>Shenyang Aviation Industry Group Co., Ltd, Shenyang 110013, China;

<sup>3</sup>Northeastern University, Shenyang 110819, China

**Abstract:** A bcc-structured  $Ti_2ZrNbV$  (at%) high entropy alloy was prepared by vacuum arc melting. The stability of the solid solution phase was studied, and the improvement of tensile property via  $V_2Zr$  phase precipitation was investigated. The results show that the homogenous solid solution phase is stable above 900 °C, and Laves phase  $V_2Zr$  easily precipitates below this temperature. The instability of the solid solution phase can be used for enhancing the  $Ti_2ZrNbV$  alloy. After solid solution and aging treatment, the tensile yield strength of the alloy can reach 1145 MPa with a promising elongation of 8.3%.

**Key words:** high entropy alloy; phase stability; aging; precipitation strengthening; mechanical property

High entropy alloys (HEAs) were originally designed with multiple elements to form disordered solid solution phases with high configurational entropy<sup>[1-2]</sup>. Due to the potential good performances, such as high strength, favorable ductility, positive corrosion resistance and oxidation resistance<sup>[3-6]</sup>, HEAs have attracted extensive attention in the last decade. It is found that as compared with fcc-structured HEA, bcc-structured HEA has a higher yield strength, but its tensile elongation (EL) is usually lower<sup>[7]</sup>. Therefore, the “trade off” problem that limits the potential application of bcc-HEA is usually of importance in the research field.

Generally,  $TiZrHf(Mo)NbTa$ ,  $TiZrCrHf(V)Nb$  and  $MoNbTaVW$  composition systems are often selected for designing bcc-HEAs<sup>[7-18]</sup>. The compressive yield strength of these alloys ranges from 918 MPa to 2035 MPa, and the compressive ductility ranges from 3% to over 50%. The ductility drastically drops when the strength is high. For the equimolar  $HfNbTaTiZr$  alloy, a tensile property with the yield strength of 1145 MPa and the elongation of 9.7% can be obtained by hot-isostatic-pressing<sup>[18]</sup>. This is a promising result of bcc-HEAs at present, but it is only similar to some  $\beta$  titanium alloys.

Ti, Zr and V metals have low or medium densities. They are favorable for composing a high specific-strength HEA. The atomic radius ratio of Ti and Nb is between that of Zr and V,

which is conducive to reduce the lattice distortion of  $TiZrVNb$  system alloys. So  $TiZrVNb$  composition systems have attracted some attention in the HEA research field. Chen et al<sup>[19]</sup> designed a  $V_{0.5}Nb_{0.5}ZrTi$  alloy. It was found that the yield strength reaches to 787 MPa and the tensile elongation reaches to 21.9% after homogenization. Huang et al<sup>[20]</sup> studied the microstructures and properties of the as-cast  $Ti_xZrNbV$  ( $x=1, 1.5, 2$ ) alloys. The results showed that when  $x=1$ , the alloy is composed of the bcc-structured solid solution phase and the  $V_2Zr$  phase. When  $x=1.5$  or  $x=2$ , the alloys contain the single solid solution phase. The yield strength of the equimolar ( $x=1$ )  $TiZrNbV$  alloy is 1146 MPa, but the tensile elongation is only 3.5%. In contrast, the yield strength of the  $Ti_2ZrNbV$  alloy is 1058 MPa and the elongation is 12.3%. The above results indicate that the microstructure of  $TiZrVNb$  system alloy is closely related to Ti concentration. However, it rises up with a question: when single solid solution phase is formed in a  $TiZrNbV$  system alloy (for instance,  $Ti_2ZrNbV$ ), is the phase stable when kept at a certain temperature for a certain period of time? Although the as-cast  $Ti_2ZrNbV$  alloy contains single solid solution phase, the phase stability is unclear. If the solid solution phase is instable, the  $V_2Zr$  phase will easily precipitates during the alloy processing. It is of significance to investigate the effect of  $V_2Zr$  phase precipitation on strengthening of the alloy. In this study, the  $Ti_2ZrNbV$  (at%)

Received date: November 21, 2021

Foundation item: National Natural Science Foundation of China (51371121)

Corresponding author: Wu Baolin, Ph. D., Professor, Material Science and Engineering School, Shenyang Aerospace University, Shenyang 110036, P. R. China, Tel: 0086-24-89724198, E-mail: wubaolin@sau.edu.cn

Copyright © 2023, Northwest Institute for Nonferrous Metal Research. Published by Science Press. All rights reserved.

alloy was prepared, and the stability of the solid solution phase was studied. In addition, the property improvement via  $V_2Zr$  phase precipitation was investigated and discussed. The results provide a reference for enhancing bcc-structured HEA with a promising comprehensive mechanical property.

## 1 Experiment

The raw materials used in this work were titanium, zirconium, niobium and vanadium particles with granular shape ( $\sim 3$  mm) and purities above 99.90%. The button ingots of the alloy with mass of 100 g were prepared using a high vacuum arc melting equipment. The alloy was composed of Ti, Zr, Nb and V with molar ratio of 2:1:1:1. To ensure uniform composition, each alloy ingot was melted by electromagnetic stirring for 4 times. Various samples were cut from the ingots for microstructure observation, phase identification, composition analysis, thermal-mechanical processing and mechanical property test. To homogenize the compositions and to obtain single bcc phase, the samples were held at 1100 °C for 40 h. After then, some samples were aged at 300, 400, 500, 600, 700 and 800 °C, for phase stability investigation; some samples were cold-rolled with 75% Re at room temperature, followed by recrystallization at 950 °C for 25 min, and then aged at 300 °C for 4, 8, 12, and 16 h for the investigation of aging strengthening. In heat treatment, the samples were sealed in a vacuum quartz tube when the temperature was high ( $>600$  °C), or wrapped with anti-oxidation coat when temperature was low ( $<600$  °C).

The samples for optical observation were mechanically ground with 320–3000 mesh sandpapers, and then mechanically polished. After polishing, the samples were eroded with a corrosive solution consisting of 10% HF+30%  $HNO_3$ +60%  $H_2O$ . OLYMPUSPMG3 optical microscope and JSM-6700 scanning electron microscope (SEM) were used to observe the microstructures and to analyze the compositions of the alloy. Phase identification was performed on the Ultima IV X-ray diffractometer with the scanning angle from 10° to 90°. The scanning rate was 5°/min. The tensile test was carried out on the AI-7000-LA20 universal testing machine at room temperature. The dog-bone tensile samples was 1.5 mm in thickness, 2 mm in width and 8 mm in the standard distance.

The tensile rate was 0.4 mm/min.

## 2 Results

### 2.1 Initial microstructure and tensile property

Fig. 1a shows the typical microstructure of the  $Ti_2ZrNbV$  alloy ingots observed under optical microscope. It can be seen that the microstructure exhibits dendrites. The XRD pattern (Fig. 1b) shows that four intensive diffraction peaks correspond to bcc structure, suggesting that the microstructure is mainly composed of bcc phase. However, a slight split of  $\{110\}$  and  $\{200\}$  peaks can be identified in the pattern. This is due to the segregation which results in different element concentrations between the inter-dendrite and the inner-dendrite. Therefore, there are two bcc solid solutions with different lattice parameters. In addition, the XRD pattern exhibits two faint diffraction peaks corresponding to the C15 structure, suggesting that a few Laves phase  $V_2Zr$  is possible in the as-cast alloy. The tensile yield strength of the ingot alloy reaches to 981 MPa with the elongation of 11.2% (Fig. 1c). Because the alloy is mainly single bcc solid solution phase, of which the stacking fault energy is generally high, a large amount of cross slip will take place during plastic deformation. So hardening rate is low as seen from the tensile stress-strain curve in Fig. 1c.

The above results indicate that heavy elements segregation occurs in the solidification, and the alloy consists of the governing bcc solid solution phase and the minor  $V_2Zr$  phase.

### 2.2 Microstructure development

To investigate the stability of the single solid solution phase, the alloy samples with the initial microstructure were homogenized at 1100 °C for 40 h, and then aged at different temperatures for a certain time. The microstructure development was investigated. Fig. 2 shows the SEM microstructure and the corresponding EDS maps after the homogenization. It can be seen that the microstructure consists of single solid solution phase with homogenized compositions of Ti, Zr, Nb and V.

After aging under conditions of 800 °C/2 h, 700 °C/2 h, 600 °C/2 h, 500 °C/4 h and 300 °C/10 h, homogenized single-phase is decomposed to form secondary phase with various morphologies, as seen in Fig. 3.

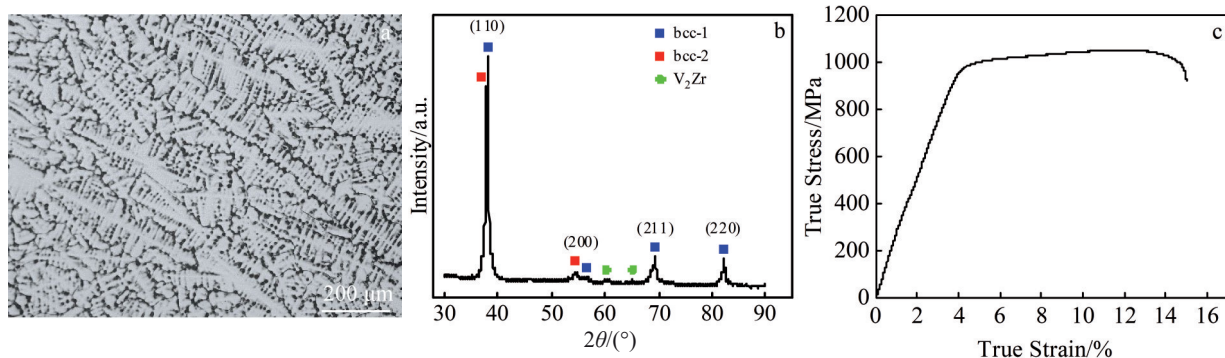


Fig.1 OM microstructure (a), XRD pattern (b) and tensile stress-strain curve (c) of as-cast  $Ti_2ZrNbV$  alloy

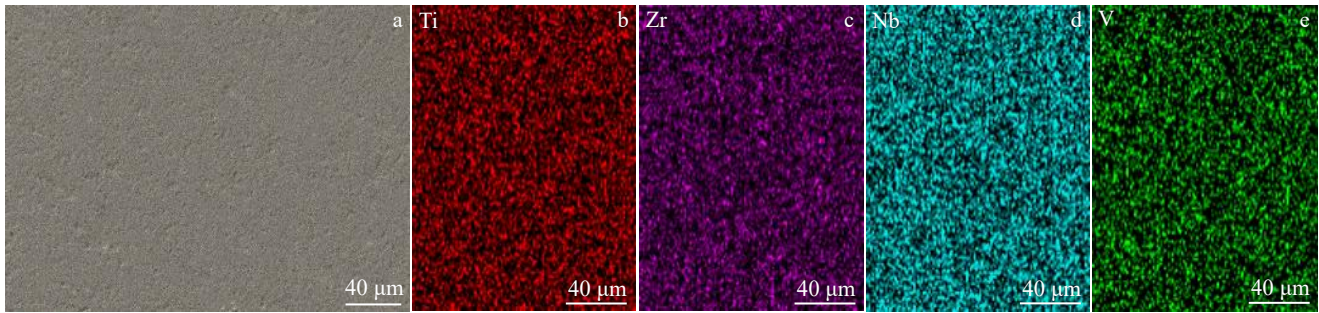


Fig.2 SEM microstructure (a) and EDS maps of element Ti (b), Zr (c), Nb (d), and V (e) of the homogenized alloy

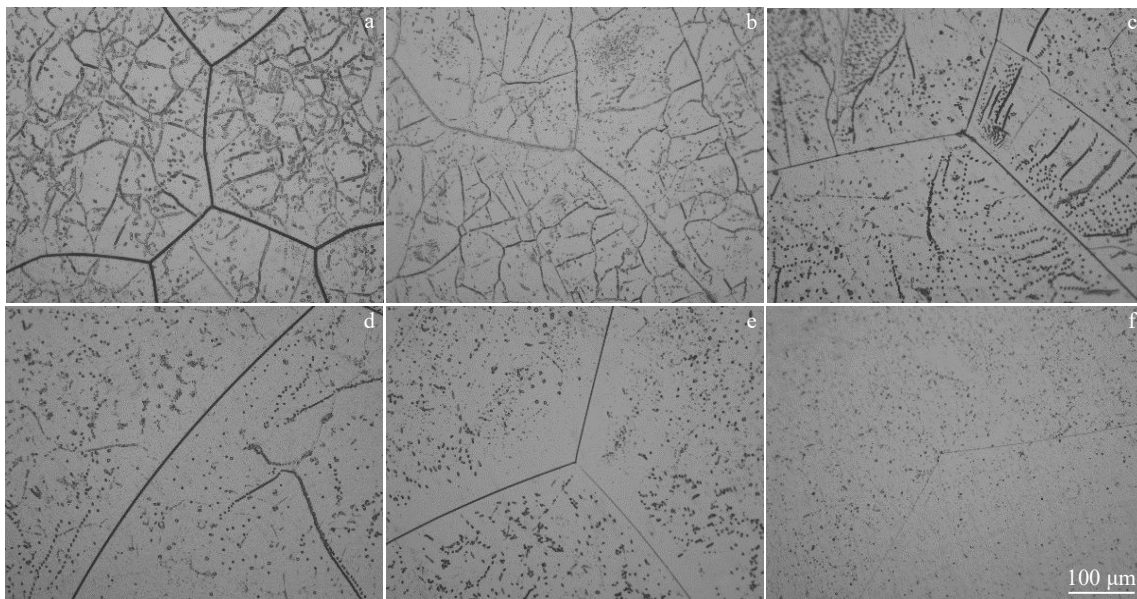


Fig.3 OM microstructures of the homogenized alloy aged under different conditions: (a) 800 °C/2 h, (b) 700 °C/2 h, (c) 600 °C/2 h, (d) 500 °C/2 h, (e) 400 °C/4 h, and (f) 300 °C/10 h

Fig. 4 shows XRD patterns of the alloy samples homogenized under 1100 °C/40 h and aged under 1100 °C/40 h+aged under 800 °C/2 h. In contrast to the homogenized sample, the aged sample exhibits additional XRD peaks corresponding to  $V_2Zr$  phase. So it is believed that the secondary  $V_2Zr$  phase precipitates from the solid solution during aging. After aging at 800 and 700 °C (Fig.3a and 3b), the  $V_2Zr$  phase exhibits a reticular morphology. When aged at 600 and 500 °C (Fig.3c and 3d), the  $V_2Zr$  phase is linearly distributed with point-like morphology. As the aging temperature decreases to 400 and 300 °C (Fig.3e and 3f), the  $V_2Zr$  phase exhibits a uniform point-like distribution in the grains, and the average size of  $V_2Zr$  particles aged at 300 °C is 1–2 μm.

### 2.3 Precipitation strengthening

Since  $V_2Zr$  phase can precipitate in a particle form at low aging temperatures, it is of significance to investigate how to use this phenomenon to strengthen the alloy. Thus, the homogenized  $Ti_2ZrNbV$  flake samples were cold-rolled with 75% reduction and then recrystallized at 950 °C for 25 min followed by quenching. The microstructure is shown in Fig.5a.

After aging at 300 °C for 4–16 h, the  $V_2Zr$  precipitation particles increase in number with increasing aging time. The corresponding OM microstructures are shown in Fig.5b–5e. It can be seen from Fig.5b and 5c that after aging for 4 and 8 h, only a few particles precipitate. When aged for 12 h (Fig.5d), precipitation phase is distributed uniformly and dispersedly in the matrix. When aged for 16 h, the precipitation particles grow up to a large size in the grains and at the grain boundaries. SEM image in Fig.5f shows the morphologies of precipitation particles (indicated by white arrows). Although the area enriched with V and Zr is not distinct in EDS maps, the EDS spectrum of the particles show approximate compositions as shown in Table 1. The stoichiometric ratio of V:Zr is nearly 2:1. Nb is probably solid-dissolved in  $V_2Zr$ . The XRD pattern of the corresponding alloy (Fig.6) shows that the diffraction peaks are characterized with  $V_2Zr$  phase, similar to Fig.4.

The precipitation has an evident influence on the tensile property, as shown in Fig.7. The yield strength of the sample processed by thermal-mechanical processing via the homogenization, cold-rolling and recrystallization is 1002

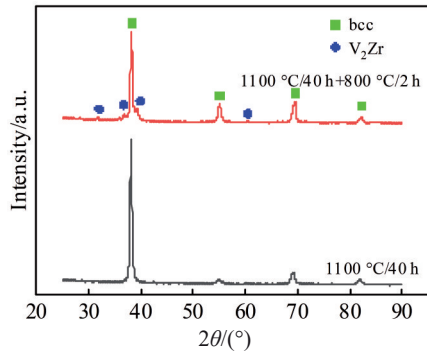


Fig.4 XRD patterns of the homogenized alloy and the aged alloy

MPa, with the corresponding elongation of 14.1%. Compared with the solidification dendrite microstructure, the microstructure via thermal-mechanical processing is highly homogeneous in composition and the strength increases. After aging for 4 and 8 h, the yield strength is 1045 and 1086 MPa

with the elongation of 10.9% and 10.4%, respectively. After aging for 12 h, the yield strength reaches to 1145 MPa with the elongation of 8.3%. The yield strength drops to 810 MPa and the elongation is only 1.7% after aging for 16 h. Compared with the recrystallized and quenched sample, the yield strength of the sample aged for 12 h is increased by 143 MPa, and the elongation is reduced by 5.8%. When the precipitates grow up inside grains and at grain boundaries (Fig.5e), the tensile property turns worse.

The above results suggest that the instability of the solid solution phase in the  $\text{Ti}_2\text{ZrNbV}$  alloy can be used for aging strengthening.

### 3 Discussion

#### 3.1 Formation of solid solution phase and its stability

To predict the formation of single solid solution phase in high entropy alloy, two parameters of  $\delta$  and  $\Omega$  were proposed<sup>[21]</sup>:

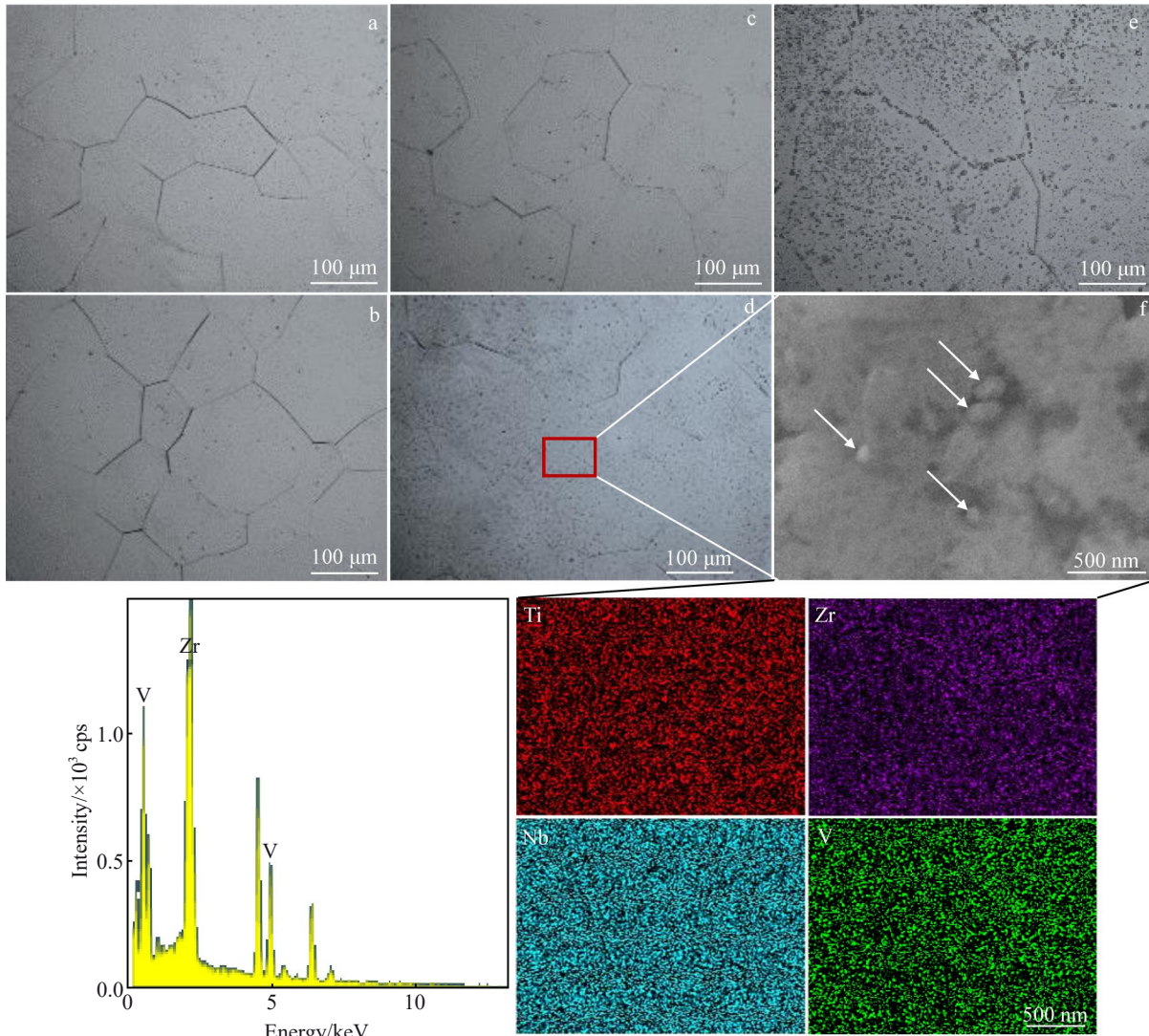


Fig.5 Microstructures of the rolled-recrystallized-quenched alloy aged at 300 °C for different time: (a) 0 h, (b) 4 h, (c) 8 h, (d, f) 12 h, and (e) 16 h; EDS spectrum of precipitation particle and EDS maps corresponding to Fig.5f

**Table 1** Approximate composition of precipitation particles of the alloy obtained by SEM-EDS (at%)

V	Zr	Nb
~63	~32	~5

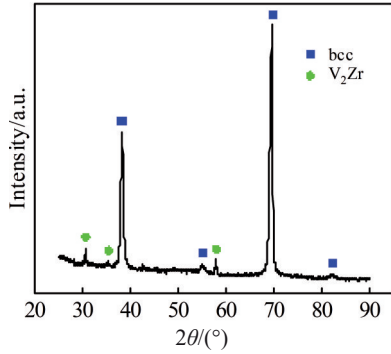


Fig. 6 XRD pattern of the rolled-recrystallized-quenched alloy aged at 300 °C for 12 h

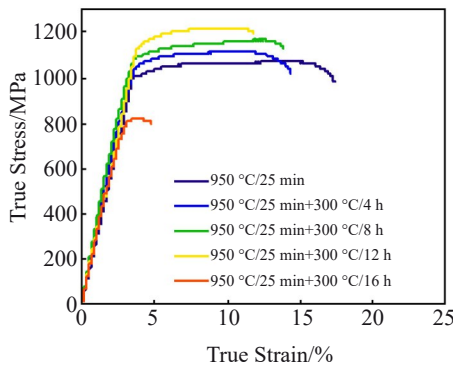


Fig. 7 True stress-true strain curves of the rolled alloy with different heat treatments

$$\delta = \sqrt{\sum_{i=1}^n c_i \left(1 - \frac{r_i}{\bar{r}}\right)^2} \quad (1)$$

$$\Omega = \frac{T\Delta S_{\text{mix}}}{|\Delta H_{\text{mix}}|} \quad (2)$$

where  $\bar{r}$  is average atomic radius of composing elements;  $c_i$  is mole fraction of the corresponding component  $i$ ;  $r_i$  is atomic radius of the corresponding element;  $T$  is thermodynamic temperature. Because the alloy begins to crystallize at melting point  $T_m$  during solidification,  $T_m$  is commonly used to replace  $T$  in the formula for calculation<sup>[21]</sup>. When the  $\delta$  value is less than 4 and the  $\Omega$  value is between 1.1 and 229.8, the alloy will completely form a bcc solid solution phase<sup>[22-25]</sup>.

In Eq. (2),  $\Delta H_{\text{mix}}$  and  $\Delta S_{\text{mix}}$  are the mixing enthalpy and mixing entropy, respectively, expressed as:

$$\Delta H_{\text{mix}} = 4 \sum_{i=1, i \neq j}^n \Delta H_{ij} c_i c_j \quad (3)$$

$$\Delta S_{\text{mix}} = -R \sum_{i=1}^n c_i \ln c_i \quad (4)$$

where  $\Delta H_{ij}$  is the mixing enthalpy of component  $i$  and component  $j$ , and  $R$  is the gas constant ( $R=8.314 \text{ J}\cdot\text{K}^{-1}\cdot\text{mol}^{-1}$ ). According to Eq. (4) and the  $\Delta H_{ij}$  table<sup>[26]</sup> where  $\Delta H_{\text{Ti-Zr}}$ ,  $\Delta H_{\text{Ti-Nb}}$ ,  $\Delta H_{\text{Ti-V}}$ ,  $\Delta H_{\text{Zr-Nb}}$ ,  $\Delta H_{\text{Zr-V}}$  and  $\Delta H_{\text{Nb-V}}$  are 0, 2, -2, 4, -4 and 1, respectively,  $\Delta H_{\text{mix}}$ ,  $\Delta S_{\text{mix}}$ ,  $\delta$  and  $\Omega$  for the  $\text{Ti}_2\text{ZrNbV}$  alloy were calculated in this study. The  $\Delta H_{\text{mix}}$  and  $\Delta S_{\text{mix}}$  values are  $-0.16 \text{ kJ/mol}$  and  $11.08 \text{ J}\cdot\text{K}^{-1}\cdot\text{mol}^{-1}$ , respectively, and the  $\delta$  and  $\Omega$  values are 0.054 67 and 151.57, respectively, meeting the criterion for the formation of single solid solution phase. In general, segregation is easy to occur when the mixing enthalpy  $\Delta H_{ij}$  value is positive, and intermetallic is easy to form when the mixing enthalpy value is negative<sup>[22]</sup>. So the segregation can be mainly induced by the Nb enrichment inside the inter-dendrite because of the positive values of  $\Delta H_{\text{Ti-Nb}}$  and  $\Delta H_{\text{Zr-Nb}}$ . Due to the negative value of mixing enthalpy  $\Delta H_{\text{Zr-V}}$ , V-Zr intermetallic potentially form. In addition, there is a large difference between the atomic radiuses of Zr and V, and electronegativity between them is high, which is also favorable for the formation of V-Zr intermetallic phase<sup>[27]</sup>. As discussed above, the solid solution phase should be metastable in the alloy and the Laves phase  $\text{V}_2\text{Zr}$  is easy to precipitate.

To discuss further, we took the Gibbs free energy criterion to theoretically predict the formation of  $\text{V}_2\text{Zr}$  phase. Gibbs free energy  $\Delta G_{\text{mix}}$  of the solid solution phase is expressed as:

$$\Delta G_{\text{mix}} = \Delta H_{\text{mix}} - T S_{\text{mix}} \quad (5)$$

If the solid solution phase is unstable, only V and Zr can form  $\text{V}_2\text{Zr}$  phase according to the present experimental result. Theoretically, we can determine the critical temperature for the phase stability via comparing the Gibbs free energy between the two states with different microstructures.

As an example, we suppose that at one of the states, a certain amount of V converts to  $\text{V}_2\text{Zr}$  at 800 °C, and the total free energy should be the sum of  $\text{V}_2\text{Zr}$  phase and the remained solid solution phase in this case. Because the  $\text{V}_2\text{Zr}$  phase is highly ordered, its  $\Delta S_{\text{mix}}$  is approximately 0. Based on calculation, the free energy of  $\text{V}_2\text{Zr}$  is  $-3.56 \text{ kJ/mol}$  if 80%V converts to  $\text{V}_2\text{Zr}$ <sup>[28]</sup>. In this case, the composition of the remained solid solution is  $\text{Ti}_2\text{Zr}_{1.2}\text{NbV}_{0.4}$ , and the free energy is  $-8.77 \text{ kJ/mol}$ . So the total free energy is  $\Delta G_{\text{mix}} = -12.33 \text{ kJ/mol}$ . Assuming that at the second state, the microstructure is composed of single solid solution phase, and its  $\Delta G_{\text{mix}}$  is  $-12.05 \text{ kJ/mol}$ .

Similarly, the free energy at the two states with different temperatures can be calculated. We obtained the development of the free energy versus temperature at two states, as resented in Fig. 8. It is seen that the free energy at the state with single solid solution phase is lower than that at the state with two-phase mixture when temperature is above 950 °C. In theory, the single-phase in the alloy is instable below 950 °C, and  $\text{V}_2\text{Zr}$  phase will precipitate. The driven force for the precipitation depends on differential free energy. This can well explain the present experiment results. The calculation result provides a theoretical support for the temperature selections of homogenization treatment (1100 °C) and recrystallization (950 °C).

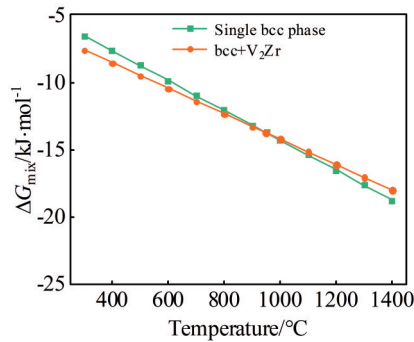


Fig.8 Calculated Gibbs free energy of the alloy with single and binary phase

### 3.2 Morphology of $V_2Zr$ precipitates

It can be seen from Fig.3 that the  $V_2Zr$  phase precipitates from the solid solution in the form of uniform point-like particles at low temperatures (300 or 400 °C). When aged at medium temperature (500 or 600 °C), the  $V_2Zr$  phase exhibits point-like and linear morphologies, and reticular morphology at high temperature (700 or 800 °C). It indicates that the morphology of the intermetallics precipitating from the solid phase transition is related to the diffusion of atoms<sup>[29, 30]</sup>. This means that the precipitation kinetics has an effect on the morphology. So the morphology of the precipitated  $V_2Zr$  phase is reticular and linear at high temperatures due to the

rapid diffusion, although the differential free energy is smaller. The differential free energy becomes larger with decreasing aging temperature (Fig.8), but the kinetic diffusion is limited. So  $V_2Zr$  phase exhibits the point-like morphology when aged at low temperatures. Fig. 9 shows the high magnification SEM images of the microstructures when aged under conditions of 600 °C/2 h, 800 °C/2 h and 900 °C/2 h. It can be seen that the reticular and linear precipitates in grains are actually composed of intermittent particles of the  $V_2Zr$  phase (Fig.9a and 9b). This suggests that the reticular and linear morphologies may be resulted from the  $V_2Zr$  particles which nucleate and grow up rapidly to link each other on the substructure defects, such as sub-grain boundaries and dislocation boundaries with network and linear shapes. For the sample aged at 900 °C, no precipitation phase is observed (Fig.9c), indicating that the solid solution phase is stable above 900 °C. This is approximately consistent with the previous theoretical calculation result.

### 3.3 Strengthening effect of $V_2Zr$ precipitates

The  $V_2Zr$  phase precipitating at medium and high temperatures is believed to have no strengthening effect because of the linear and reticular morphologies. The uniformly distributed point-like  $V_2Zr$  phase at low temperature has a certain strengthening effect as shown in the present study. After aging at 300 °C, the number of the  $V_2Zr$  phase particles is promising, and their size is not very large bcc

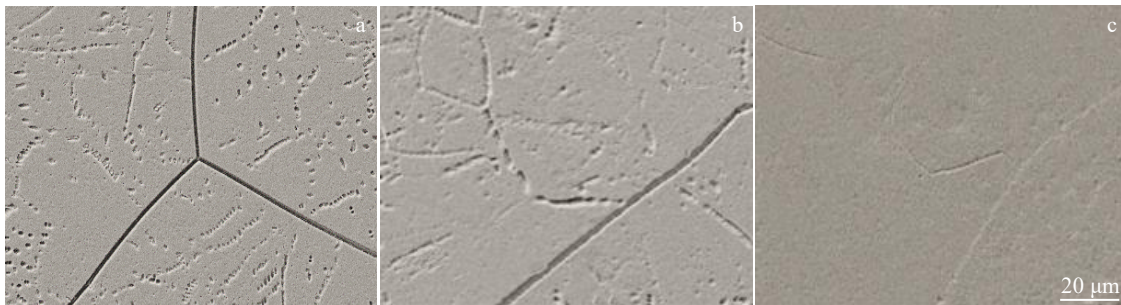


Fig.9 SEM images of homogenized alloy aged at different temperatures for 2 h: (a) 600 °C, (b) 800 °C, and (c) 900 °C

due to the low diffusion rate<sup>[31, 32]</sup>. The uniformly distributed  $V_2Zr$  particles play a role in pinning dislocations during the plastic deformation. The strengthening effect is the best when aged for 12 h and the yield strength of the alloy is as high as 1145 MPa. When the aging time is extended to 16 h, the  $V_2Zr$  phase particles grow up to large size, and some of them are at grain boundaries. This will cause serious stress concentrations during tension, and lead to a premature fracture. Therefore, the tensile property of the alloy becomes worse when aged at 300 °C for 16 h. As discussed above, it is feasible to use the  $V_2Zr$  phase precipitation to enhance the alloy via quenching and aging at 300 °C for less than 12 h.

Fig. 10 shows the comprehensive comparison of tensile yield strength and elongation between the present results and some previous results<sup>[7-8, 12, 33-37]</sup>. The properties of high-entropy

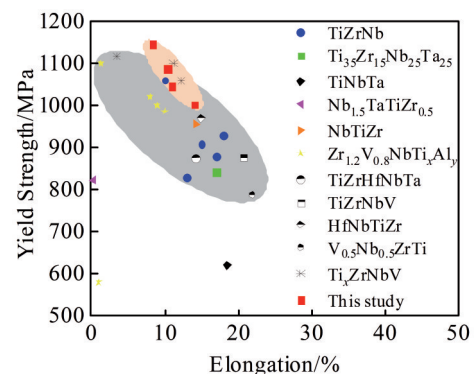


Fig.10 Comparison of comprehensive tensile yield strength and elongation between the present results and some previous results

alloys reported in the previous studies are mainly in the gray area. The present results are in the pink region. In contrast, the comprehensive tensile property of the present alloy is superior to that of the previous one. It can be concluded that strengthening through aging is an effective way to enhance the Ti<sub>2</sub>ZrVNb HEA. This provides a reference for developing bcc-structured HEAs with a promising mechanical property.

#### 4 Conclusions

1) The microstructure of as-cast Ti<sub>2</sub>ZrNbV alloy is dendritic with severe segregation. There are two kinds of solid solution phases with bcc structure in the alloy due to different element concentrations in the inter-dendrite and inner-dendrite. The tensile yield strength of as-cast alloy can reach to 981 MPa with an elongation of 11.2%.

2) The homogenous bcc solid solution with single-phase is stable above 900 °C, and Laves phase V<sub>2</sub>Zr easily precipitates from the solid solution phase when aged below this temperature. V<sub>2</sub>Zr phase nucleates and grows up rapidly at the locations of substructure defects, forming a large amount of equiaxed particles linking to each other in networks and lines when aged at 800 and 700 °C. The V<sub>2</sub>Zr phase precipitates in solid solution grains in the form of uniformly distributed point-like particles, and the average size of V<sub>2</sub>Zr particles is 1–2 μm when aged at 300 °C for 12 h.

3) The tensile yield strength of the alloy increases and the plasticity decreases with increasing aging time when aged at 300 °C for less than 12 h. The tensile yield strength can reach to 1145 MPa with a promising elongation of 8.3%. When aging time increases to 16 h, the tensile property becomes worse.

4) The instability of the solid solution phase can be used for enhancing the Ti<sub>2</sub>ZrNbV high entropy alloy.

#### References

- 1 Yeh J W, Chen S K, Lin S J et al. *Advanced Engineering Materials*[J], 2004, 6: 299
- 2 Yeh J W, Chen S K, Gan J W et al. *Metall Mater Trans A*[J], 2004, 35: 2533
- 3 Gorr B, Muller F, Azim M et al. *Oxidation of Metals*[J], 2017, 88(3–4): 339
- 4 Regenber M, Hasemann G, Wilke M et al. *Metals*[J], 2020, 10: 1530
- 5 Senkov O N, Woodward C F. *Materials Science and Engineering A*[J], 2011, 529: 311
- 6 Jiang Honglin, Hu Zhifang, Yuan Xuetao et al. *Rare Metal Materials and Engineering*[J], 2020, 49(8): 2820 (in Chinese)
- 7 Fazakas É, Zadorozhnyy V, Varga L K et al. *International Journal of Refractory Metals and Hard Materials*[J], 2014, 47: 131
- 8 Senkov O N, Wilks G B, Scott J M et al. *Intermetallics*[J], 2011, 19(5): 698
- 9 Senkov O N, Senkova S V, Woodward C et al. *Acta Materialia*[J], 2013, 61(5): 1545
- 10 Senkov O N, Senkova S V, Woodward C. *Acta Materialia*[J], 2014, 68: 214
- 11 Senkov O N, Woodward C, Miracle D B. *JOM*[J], 2014, 66(10): 2030
- 12 Wu Y D, Cai Y H, Wang T et al. *Materials Letters*[J], 2014, 130: 277
- 13 Yang X, Zhang Y, Liaw P K. *Procedia Engineering*[J], 2012, 36: 292
- 14 Stepanov N D, Shaysultanov D G, Salishchev G A et al. *Materials Letters*[J], 2015, 142: 153
- 15 Guo N N, Wang L, Luo L S et al. *Materials & Design*[J], 2015, 81: 87
- 16 Senkov O N, Scott J M, Senkova S V et al. *Journal of Materials Science*[J], 2012, 47(9): 4062
- 17 Senkov O N, Senkova S V, Miracle D B et al. *Materials Science and Engineering A*[J], 2013, 565: 51
- 18 Senkov O N, Semiatin S L. *Journal of Alloys and Compounds*[J], 2015, 649: 1110
- 19 Chen Y, Xu Z, Wang M et al. *Materials Science and Engineering A*[J], 2020, 792: 139 774
- 20 Huang T, Wu S, Jiang H et al. *International Journal of Minerals, Metallurgy and Materials*[J], 2020, 27(10): 1318
- 21 Klimenko D N, Yurchenko N Y, Stepanov N D et al. *Materials Today: Proceedings*[J], 2021, 38: 1535
- 22 Yang X, Zhang Y. *Materials Chemistry and Physics*[J], 2012, 132(2–3): 233
- 23 Wang Z, Guo S, Liu C T. *JOM*[J], 2014, 66(10): 1966.
- 24 Zhang Y, Zhou Y. *Materials Science Forum*[J], 2007, 561–565: 1337
- 25 Guo S, Liu C T. *Progress in Natural Science: Materials International*[J], 2011, 21(6): 433
- 26 Akira T, Akihisa I. *Materials Transactions*[J], 2005, 46: 2817
- 27 King D J M, Cheung S T Y, Humphry Baker S A et al. *Acta Materialia*[J], 2019, 166: 435
- 28 Feuerbacher M, Lienig T, Thomas C. *Scripta Materialia*[J], 2018, 152: 40
- 29 Fisher K, Barron S C, Bonds M A et al. *Journal of Applied Physics*[J], 2013, 114(24): 258 898
- 30 Fei Q. *Chinese Journal of Solid Mechanics*[J], 2012, 33(2): 1
- 31 Murakami T, Too V C W S. *Solid State Technology*[J], 2003, 46(9): 32
- 32 Medved I, Trnik A. *Physical Review E*[J], 2012, 86(1): 11601
- 33 Wang S, Wu M, Shu D et al. *Acta Materialia*[J], 2020, 201: 517
- 34 Wang J, Bai S, Tang Y et al. *Journal of Alloys and Compounds*[J], 2021, 868: 159 190
- 35 Wang L, Chen S, Li B et al. *Materials Science and Engineering A*[J], 2021, 814: 141 234
- 36 Mustafi L, Nguyen V T, Lu S L et al. *Materials Science and Engineering A*[J], 2021, 824: 141 805
- 37 Zyka J, Malek J, Vesely J et al. *Entropy (Basel)* [J], 2019, 21(2): 114

## Ti<sub>2</sub>ZrNbV 高熵合金的相稳定性和时效强化

李健博<sup>1</sup>, 万刚<sup>1</sup>, 吴波<sup>2</sup>, 徐再东<sup>1</sup>, 满佳乐<sup>3</sup>, 张璐<sup>1</sup>, 武保林<sup>1</sup>

(1. 沈阳航空航天大学, 辽宁 沈阳 110036)

(2. 沈阳航空产业集团公司, 辽宁 沈阳 110013)

(3. 东北大学, 辽宁 沈阳 110819)

**摘要:** 采用真空电弧熔炼法制备了具有体心立方结构的Ti<sub>2</sub>ZrNbV (at%) 高熵合金。研究了固溶体相的稳定性, 以及金属间化合物V<sub>2</sub>Zr析出对拉伸性能的改善。结果表明: 合金在900 °C以上是稳定单一均质固溶体相, 低于此温度时, Laves相V<sub>2</sub>Zr容易在基体中析出。单一固溶相的不稳定性可用于强化Ti<sub>2</sub>ZrNbV高熵合金。经过固溶和时效处理后, 合金的拉伸屈服强度可达1145 MPa, 塑性伸长率为8.3%。

**关键词:** 高熵合金; 相稳定性; 时效; 沉淀强化; 机械性能

---

作者简介: 李健博, 男, 1998年生, 硕士, 沈阳航空航天大学材料学院, 辽宁 沈阳 110036, 电话: 024-89724198, E-mail: wubaolin@sau.edu.cn